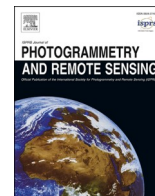


Contents lists available at [ScienceDirect](https://www.sciencedirect.com)

ISPRS Journal of Photogrammetry and Remote Sensing

journal homepage: www.elsevier.com/locate/isprsjprs

Multisensor approach to land use and land cover mapping in Brazilian Amazon

Victor Hugo Rohden Prudente^{a,b,*}, Sergii Skakun^{b,c}, Lucas Volochen Oldoni^a,
Haron A. M. Xaud^d, Maristela R. Xaud^d, Marcos Adami^a, Ieda Del'Arco Sanches^a

^a Earth Observation and Geoinformatics Division, National Institute for Space Research, Sao Jose dos Campos, SP 12227-010, Brazil

^b Department of Geographical Sciences, University of Maryland, College Park, MD 20742, USA

^c NASA Goddard Space Flight Center Code 619, Greenbelt, MD 20771, USA

^d Embrapa Roraima, Brazilian Agricultural Research Corporation, Boa Vista, RR 69301-970, Brazil

ARTICLE INFO

Keywords:

Classification
Sentinel images
Random Forest
Multilayer Perceptron
t-Distributed Stochastic Neighbor Embedding
Roraima state

ABSTRACT

Remote sensing has an important role in the Land Use and Land Cover (LULC) mapping process worldwide. Combining spaceborne optical and microwave data is essential for accurate classification in areas with frequent cloud cover, such as tropical regions. In this study, we investigate the possible improvements, when SAR data is incorporated into the classification process along with optical data. We used MSI/Sentinel-2 and SAR/Sentinel-1 to provide LULC mapping in the Roraima State, Brazil, in 2019. This State is located in a tropical area, where the cloud cover is frequent over the year. Cloud cover becomes substantial, especially during the May–August period when crops are grown. Twenty-nine scenarios involving a combination of optical- and SAR-based features, as well as times of data acquisition, were considered in this study. Our results showed that optical or SAR data used individually are not enough to provide accurate LULC mapping. The best results in terms of overall accuracy (OA) were achieved using metrics of multi-temporal surface reflectance and vegetation index (VI) for optical imagery, and values of backscatter coefficient in different polarizations and their ratios yielding an OA of $86.41 \pm 1.74\%$. Analysis of three periods of data (January to April, May to August, and September to December) used for classification allowed us to identify the optimal period for distinguishing specific classes. When comparing our LULC map with a LULC product derived within the MapBiomass project we observed that our method performed better to map annual and perennial crops and water classes. Our methodology provides a more accurate LULC for the Roraima State, and the proposed technique can be applied to benefit other regions that are affected by persistent cloud cover.

1. Introduction

Nowadays, combining food production while minimizing the environmental impact is one of the biggest challenges to be faced by the agriculture sector, government, and researchers (Estes et al., 2016; Searchinger et al., 2015). Although part of this food demand is met by agriculture expansion resulting in severe environmental impacts (Lambin et al., 2003) and contributing to global climatic changes (Deng et al., 2013). In this sense, continuing Land Use and Land Cover (LULC) mapping is fundamental to land use management and to understand the environmental effects at local, regional, and global scales (Adami et al., 2018; Pavanelli et al., 2018). Thus, Remote Sensing (RS) technology is widely utilized for synoptic and continuous LULC monitoring, allowing

identification of the LULC Changes (LULCC) (Veloso et al., 2017; Wulder et al., 2015).

Traditionally, optical RS (ORS) data is used to map and characterize LULC, but it suffers from limitations due to cloud cover (Asner, 2001; Martins et al., 2018; Wulder et al., 2015). High cloud frequency is a persistent characteristic found in the Amazon region, which highly compromises LULC mapping based on ORS data (Martins et al., 2018; Prudente et al., 2020a), especially in agricultural areas whose growth occurs during the rainy season (Prudente et al., 2020a). Cloud cover along with landscapes fragmentations and transitions among vegetation types (Laurin et al., 2013; Lu et al., 2012) and rapid LULCC (Eberhardt et al., 2016; Whitcraft et al., 2015) make the use of ORS data challenging to map LULC in Amazon regions (Eberhardt et al., 2016;

* Corresponding author.

E-mail address: victor.rohden@yahoo.com (V.H.R. Prudente).

<https://doi.org/10.1016/j.isprsjprs.2022.04.025>

Received 10 July 2021; Received in revised form 18 April 2022; Accepted 26 April 2022

Available online 13 May 2022

0924-2716/© 2022 International Society for Photogrammetry and Remote Sensing, Inc. (ISPRS). Published by Elsevier B.V. All rights reserved.

Sano et al., 2007; Whitcraft et al., 2015; Zhang et al., 2020).

One approach to overcome the cloud cover limitation is the use of Synthetic Aperture Radar (SAR) (Whitcraft et al., 2016). SAR sensors can provide useful data in almost all-weather conditions, independent of sunlight illumination, being less influenced by cloud cover frequency than optical data (Cué La Rosa et al., 2019; Liu et al., 2013; Moreira et al., 2013; Wulder et al., 2015). SAR signal interacts with the surface differently compared to optical data and depends on surface factors, such as dielectric constant, geometry, topography and surface roughness, and radar system parameters, such as polarization, frequency, and incident angle (Harfenmeister et al., 2019; Steele-Dunne et al., 2017). Sentinel-1 SAR provides open and high temporal frequency data and can be used to improve and/or develop new methods for mapping and monitoring LULC (Tamm et al., 2016). However, since SAR data interpretation is complex, its use is not widespread as ORS data (Oldoni et al., 2020).

Thus, approaches that integrated both optical and SAR data have been explored in LULC studies, allowing to take advantage of each sensor (Clerici et al., 2017; Inglada et al., 2016; Reiche et al., 2018; Torbick et al., 2017a; Van Tricht et al., 2018). Optical data represents the reflectance from the topmost layer of the canopy, meanwhile, the SAR data represents canopy geometric information (Joshi et al., 2016; Laurin et al., 2013). However, the methods to integrate the optical and SAR multisensor data are specific and complex (Wulder et al., 2015). The integration between optical and SAR data can be performed at the pixel (data fusion), feature, and decision levels (Joshi et al., 2016; Pohl and Van Genderen, 1998; Reiche et al., 2013). Data fusion consists of methods that generate a third image from the merged input images, i.e. fusion process, which is less common for the SAR-optical approach (Nasirzadehdizaji et al., 2019; Wulder et al., 2015), due to the disparate characteristics between the SAR and optical sensors (Wulder et al., 2015). For the decision level, SAR and optical data are independently classified and combined in a post-classification process (Reiche et al., 2013). Feature fusion requires the extraction of features, or characteristics, from the input optical and SAR data (Reiche et al., 2013) and combining these data as inputs in a dataset for the different post-processing purposes (Nasirzadehdizaji et al., 2019). Feature level is more traditional to the SAR and optical approaches (Nasirzadehdizaji et al., 2019; Reiche et al., 2013).

Two commonly used LULC classification algorithms are Random Forest (RF) (Breiman, 2001) and Multilayer Perceptron (MLP) (Burger et al., 2012). The RF classifier is highlighted due to the robustness and capability to hold a high number of variables (Diniz et al., 2020; Jhonnerie et al., 2015), and high data dimensionality (Torbick et al., 2017b) has been used in different LULC studies (Clerici et al., 2017; Inglada et al., 2016; Pavanelli et al., 2018; Rodriguez-Galiano et al., 2012; Torbick et al., 2017a, 2017b, 2016; Zhou et al., 2017). Meanwhile, the MLP is a feed-forward artificial neural network (NN) trained by the backpropagation method, designed to map a set of input vectors to a set of output vectors (Camargo et al., 2019; Hu et al., 2019; Skakun et al., 2016). These classifiers can combine the SAR and optical data at the feature level (Clerici et al., 2017; Lu et al., 2012).

Even though LULC map information is highly important for the management of tropical areas, there is a lack of information for some regions in the Brazilian Amazon. Regions of Savanna and Campinarana vegetation are not considered in programs designed for forest monitoring despite their ecological importance (Carvalho and Mustin, 2017). In this context, this study aims to classify the LULC in a tropical area in Roraima State, in the Brazilian Amazon region, providing a robust methodology to fill this gap of information. We have investigated the benefits of combining SAR with optical data in the LULC mapping process. In our study, we used RF and the MLP classifiers and Sentinel-1 SAR and Sentinel-2 MSI (Multispectral Instrument) optical images acquired in different periods of 2019.

2. Material and methods

This section is divided into five sub-sections. In section 2.1 we describe the study area and the fieldwork to collect field observation data. In section 2.2, we present remote sensing data and the pre-processing steps. The experimental setup with multiple scenarios tested is described in section 2.3. Finally, in sections 2.4 and 2.5, we focus on multi-dimension feature visualization using the t-SNE approach (t-Distributed Stochastic Neighbor Embedding), and LULC classification, respectively. Fig. 1 shows an overall flowchart describing the various steps.

2.1. Study area and fieldwork

Roraima State located in the northern part of Brazil (Fig. 2) has an area of 224,300 km², is composed of 15 municipalities, and has a population of 606,000 (IBGE, 2018). The Roraima region has three major natural formations: Forest, Savanna (also called the “lavrado”), and Campinarana (or campina-campinarana) (Barbosa et al., 2010). The main part of Roraima State is covered by forests with concentration at the center-southern part and divided into Seasonal Semideciduous Forest, Seasonal Forest, Open, and Dense Ombrophilous Forest. Savanna and Steppe Savanna are mostly present in the northern part of Roraima State. These classes have grasslands and few arbutus trees (Barbosa et al., 2010; Pavanelli et al., 2018). Campinarana is present in the center-southern part (in the middle of the forest region). It is formed by campinas (with small arbutus trees) and campinarana. Some regions show ecologic tension, where the transition between two or more types of vegetation occurs, such as Savannas and Forest, and Campinarana and Forest (Barbosa et al., 2010; Barbosa and Bacelar-Lima, 2008; IBGE, 2012).

Roraima is located in a region where the altitude ranges from 30 m in the Negro River to almost 3,000 m in the Roraima mountain (Barbosa and Bacelar-Lima, 2008). The altitude range act as a natural barrier blocking the moisture brought by the trade winds along the Intertropical Convergence Zone (ITCZ). This generates a precipitation gradient and a high cloud frequency in the region, which greatly limits the use of satellite optical images. Barni et al. (2020a) describe that Roraima has two well-defined climatic seasons, but it is different in the areas of the state located in the north from the areas in the southern hemisphere. Most of the Roraima territory has rainy seasons concentrated between April to September, with a peak in June. In the lavrados, the small lakes fill and connect in this period. The mean annual temperature is 28 °C (Pavanelli et al., 2018).

Climatic and altitude factors, water availability, as well as affordable land prices, and government subsidies, have encouraged agricultural exploitation (agriculture and livestock) in the state (Roraima, 2018). Moreover, the crop calendar for the main crops (i.e. soybean and the first season of corn) with harvest occurring during the off-season of the other Brazilian states (April-September) favors better prices and facilitates the production chain logistics. Besides, agriculture in Roraima is in the process of expansion mainly over the lavrados, especially after 2010, due to the soybean crop expansion.

For our study, we selected an area located near ecological tension between savannas and forests (Fig. 2). We selected this area due to the LULC heterogeneity, ecologic tension, and presence of agricultural lands. To provide accurate information about the LULC classes we conducted fieldwork campaigns in August-September 2019 during the agricultural season and the end of the rainy season. Using the Locus Map Pro (Mlavec and Mlavcová, 2019) application, we navigated and collected LULC roadside samples (points). Those points were used as a guide to drawing polygons using 10-m Sentinel-2 images as a background. These polygons were used as our field samples. For the study area (Fig. 2), we used 719 polygons, representing 10 LULC classes: forest, savanna, campinarana, water, sand/rock, annual crops, perennial crops, pasture, conversion, impermeable (see Fig. 3).

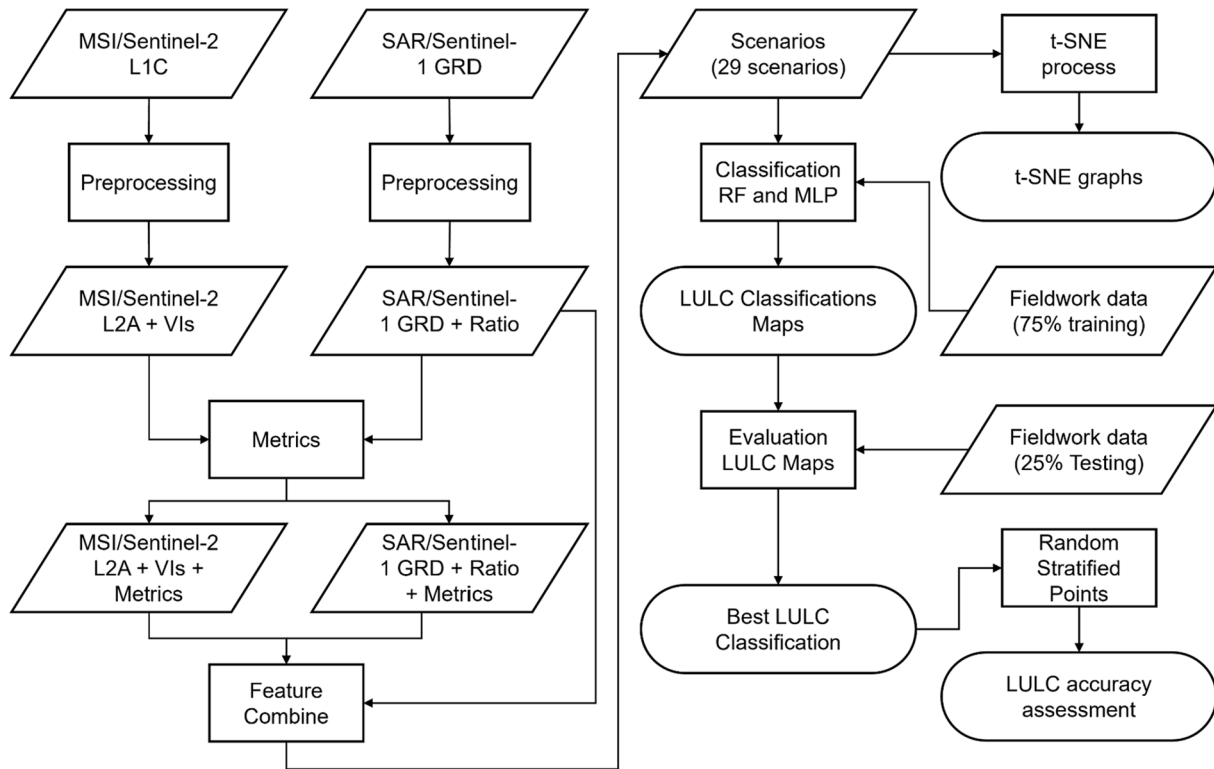


Fig. 1. Flowchart showing the processing steps.

2.2. Remote sensing data

We used images acquired by Sentinel-2 MSI over tiles 20NQJ and 20NQH, and Sentinel-1 SAR. Images were obtained from the Copernicus Open Access Hub (also known as the Sentinels Scientific Data Hub) (<https://scihub.copernicus.eu/>) using an open-source toolbox SentinelSat (<https://github.com/sentinelsat/sentinelsat>) (Hu et al., 2018).

Due to the frequent cloud cover, which mainly occurs during the crop season, it is nearly impossible to obtain cloud-free optical data in this region (Pavanelli et al., 2018; Prudente et al., 2020a). We acquired optical images with less than 70% of cloud cover totaling 23 images from Sentinel-2A/B for 2019 (Fig. 4). The optical data was downloaded at Level-1C (top-of-atmosphere reflectance). We used the bands Blue, Green, Red, Red-edge 1, Red-edge 2, Red-edge 3, Near-Infrared (NIR), Near-Infrared Narrow (NIR-A), Shortwave Infrared 1 (SWIR 1), and Shortwave infrared 2 (SWIR 2) (ESA, 2020). We applied atmospheric correction, cloud masking, and multi-temporal co-registration. The atmospheric correction was performed with the Sen2Cor algorithm (v2.8available in the SNAP software). Cloud masking was performed using Fmask v4.0 software (Qiu et al., 2019).

After the atmospheric correction and cloud cover mask, we resampled 20-m spectral bands to 10 m using the nearest neighbor resampling method. The image with the fewest cloud cover percentage acquired on April 1, 2019, was selected as a reference to corregister all other images, using a phase correlation approach (Skakun et al., 2017). We also calculated two Vegetation Indices (VIs), namely NDVI (Normalized Difference Vegetation Index) (Rouse et al., 1973) and LSWI (Land Surface Water Index) (Xiao et al., 2004, 2002). The NDVI is one of the most known VI and is associated with vegetative vigor. LSWI is sensitive to the water presence and is used for flood mapping (Dong et al., 2013; Torbick et al., 2016). NDVI (Equation (1)) and LSWI (Equation (2)) equations are presented in the following:

$$NDVI = \frac{NIR - Red}{NIR + Red} \quad (1)$$

$$LSWI = \frac{NIR - SWIR}{NIR + SWIR} \quad (2)$$

where NIR (near-infrared region, MSI/band 8–842 nm), Red (visible region, MSI/band 4–665 nm), and SWIR (shortwave infrared region, MSI/band 11–1610 nm), are surface reflectance in each spectrum region.

As SAR data sources we used Sentinel-1A and 1B (Torres et al., 2012) GRD (Ground Range Detected) images acquired in VH/VV polarizations in the IW (Interferometric Wide swath) mode. Sentinel-1 has a temporal resolution of 12 days for each satellite, and 4 and 8 days considering both satellites. In total, we used 59 Sentinel-1 images for 2019. The preprocessing was performed using the Sentinel Application Platform-SNAP applications and python routines. To define the preprocessing steps, we ran several tests to adapt the methods proposed by Dey et al. (2020). Our preprocessing included: application of orbit file; thermal noise removal without re-introduction; calibration to gamma nought; multi-looking; speckle filtering using refined Lee algorithm with windows size 3x3; terrain correction with bilinear resampling method to 10 m; conversion pixel values to decibels (dB). We also calculated the ratio between polarizations VH and VV (Equation (3)). The ratio is less affected by environmental factors or acquisition systems, thus might have more stability than single polarizations VH or VV (Harfenmeister et al., 2019; Veloso et al., 2017).

$$Ratio = \frac{VH}{VV} \quad (3)$$

2.3. Scenarios for LULC classification

To analyze the SAR data influence on the LULC classification process, we aggregated Sentinel-1 and Sentinel-2 data into four different input data (Table 1) and combined these data in six different datasets (Table 2). For the input data, we used different metrics to explore the temporal variation from the data: average, median, standard deviation, variance, range, and percentiles (25%, and 75%) metrics for optical

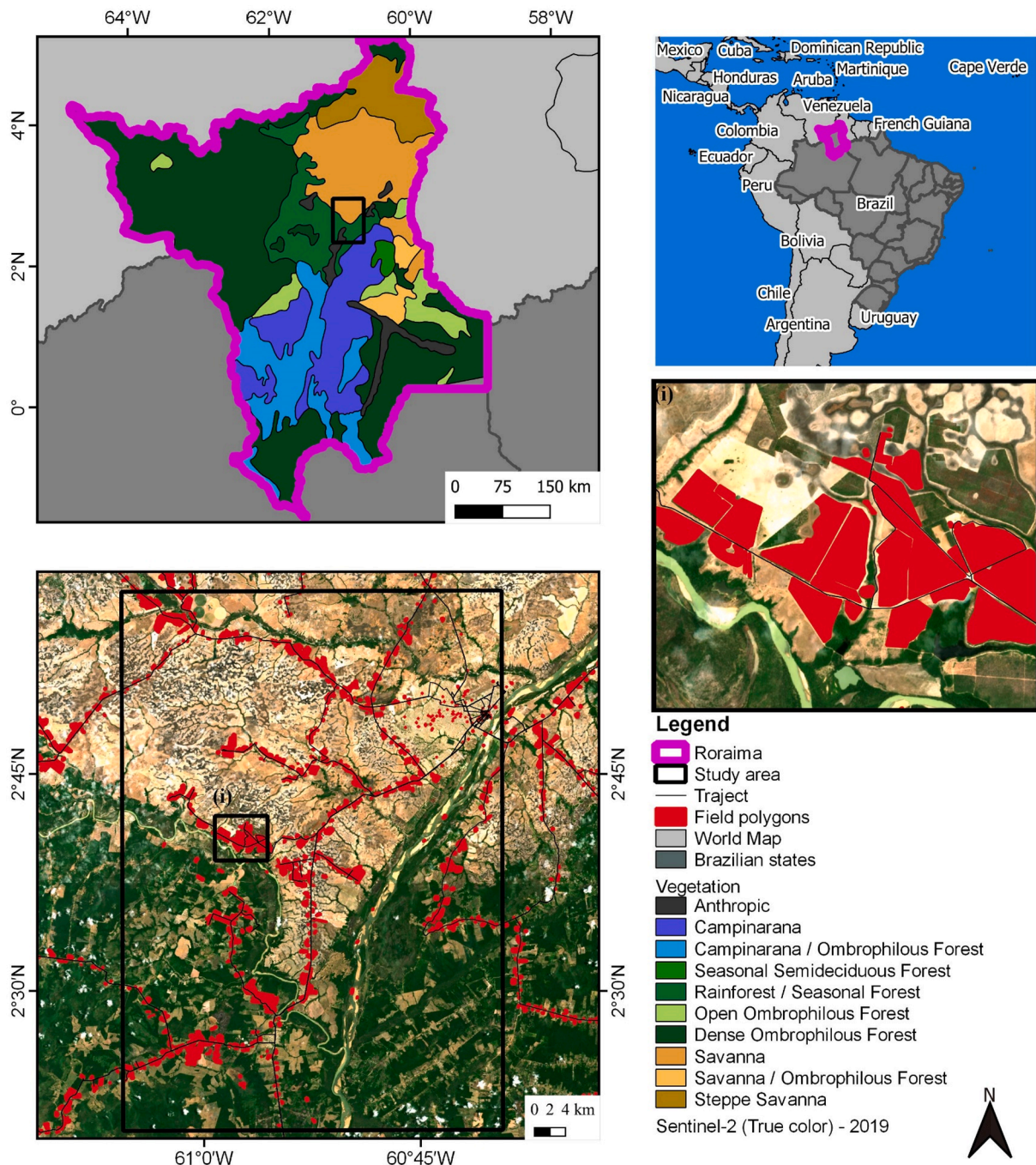


Fig. 2. Roraima state location with Vegetation Map (Barbosa and Bacelar-Lima, 2008; IBGE, 2012) and study area with fieldwork detail, 2019 Sentinel-2 RGB True color image, using mean of the band values over the year (right-bottom).

(surface reflectance and VI) and SAR (backscattering and ratio) data. For this step, we used the Pandas (The pandas development team, 2020) and Numpy (Harris et al., 2020) libraries in the python routine. Due to the different incidence angles from Sentinel-1A and 1B interfering in the backscattering values, we proceed with metrics separately.

As datasets (Table 2), we combined the input data (Table 1) in optical only data (D1 and D2), optical and SAR data combined (D3 and D4), and SAR data only (D5 and D6). For optical data, we used metrics instead of single optical images to minimize cloud influence. We performed the integration between SAR and optical data at feature levels (Gómez, 2017; Inglada et al., 2016; Pavanelli et al., 2018; Skakun et al., 2016; Zhang et al., 2018). We assumed that there is no consistent shift between the SAR and the optical images.

We divided the year into three different periods: Period 1 – P1 (January to April), Period 2 – P2 (May to August), Period 3 – P3 (September to December), Period 4 – P4 (data for the whole year), and Period 5 – P5 (the periods P1, P2, and P3 combined). P1 and P3 represent the dry periods. P2 represents the rain season when annual crops are present in Roraima. We combined P1, P2, and P3 into the P5 to represent the seasonal variation from each period. P4 represents the data for the whole year (January to December), without considering the variation within each period. Combining the different periods with the datasets, we created 29 different scenarios (Table 2). P4 is equal to P5 only for D6. This is because we did not use any metrics (average, median, standard deviation, variance, range, and percentiles (25%, and 75%)), in this dataset. Consequently, we did not have the periods

		
Forest: Natural tree formations. This class has Forest, Buriti, and parkland cerrado.	Savanna: Savannas, including clean, dirty, and cerrado field	Campinarana: Campinas and campinarana.
		
Water: Water formations, such as lakes, rivers, and dams.	Sand/rocks: Sandbank and outcrop.	Annual Crops: Areas that are used for temporary crops. It was identified soybean, corn, beans, rice, fallow land, and other annual crops
		
Perennial Crops: Perennial crops and/or silviculture. We identified Acacia, Papaya, Cashew, Dende, Mango	Pasture: Class with cultivated pasture	Conversion: Areas in conversion during the 2019 year. Areas that were being converted from natural formations to something else, during the fieldwork.
		
Impermeable: This class has urban areas, roads, and other buildings.		

Fig. 3. Land Use and Land Cover classes description with field photos.

separation (P1, P2, and P3) for this dataset. For this reason, it was not considered the P5 period.

2.4. t-SNE

t-SNE (t-Distributed Stochastic Neighbor Embedding) is a technique to visualize the separation among the classes. This approach can be used to understand if the high dimensional dataset can or cannot provide separability among the classes (Maaten, 2014; Van Der Maaten and Hinton, 2008). Although the t-SNE technique is not widely used in the remote sensing field, it seems very promising. Dey et al. (2020) used t-SNE to visualize the separation among different crop classes using polarimetric SAR data, and Martins et al. (2020) to visualize the features learned by Deep Neural Network (DNN) in each hidden layer. We used the t-SNE technique to reduce our high dimensionality data allowing us to understand the possibility of class separation before the classification process (exploratory analysis). If there is no separability among the classes there will be no point in testing several classification scenarios. We used t-SNE from the scikit-learn library (Pedregosa et al., 2011) with the number of iterations for optimization set to 300, and perplexity, the number of nearest neighbors that are used in other manifold learning algorithms, was set to 30.

2.5. Classification methods

We used two machine learning classifiers in this study: Random Forest (RF) and Multi-Layer Perception (MLP), using a python routine with the scikit-learn library (Pedregosa et al., 2011). After testing different parameters (Prudente et al., 2020b), we used numbers of trees equal to 30, no maximum depth of the tree, no maximum number of features and minimum split samples equal to 2 to the RF classifier, and one hidden layer with size equal to 50, rectified linear unit as activation function, stochastic gradient-based optimizer, alpha (L2 regularization) equal to 0.01, and learning rate values of 0.005 for the MLP classifier. The field data (polygons), section 2.1, were randomly separated into 75% for training and 25% to test which classification had the results that best fit the data collected in the field (testing data). This separation was performed for each class, and all the pixels values inside each polygon were used. We also guarantee that a polygon was used only for training or only for testing. For the accuracy assessment and selection of the best LULC classification, we analyzed the confusion matrix, the overall accuracy (OA), user’s accuracy (UA), and producer’s accuracy (PA) (Olofsson et al., 2014). To compare the results among the scenarios for each classifier, we randomly selected samples from our field data and used them to estimate the OA confidence interval based on the standard

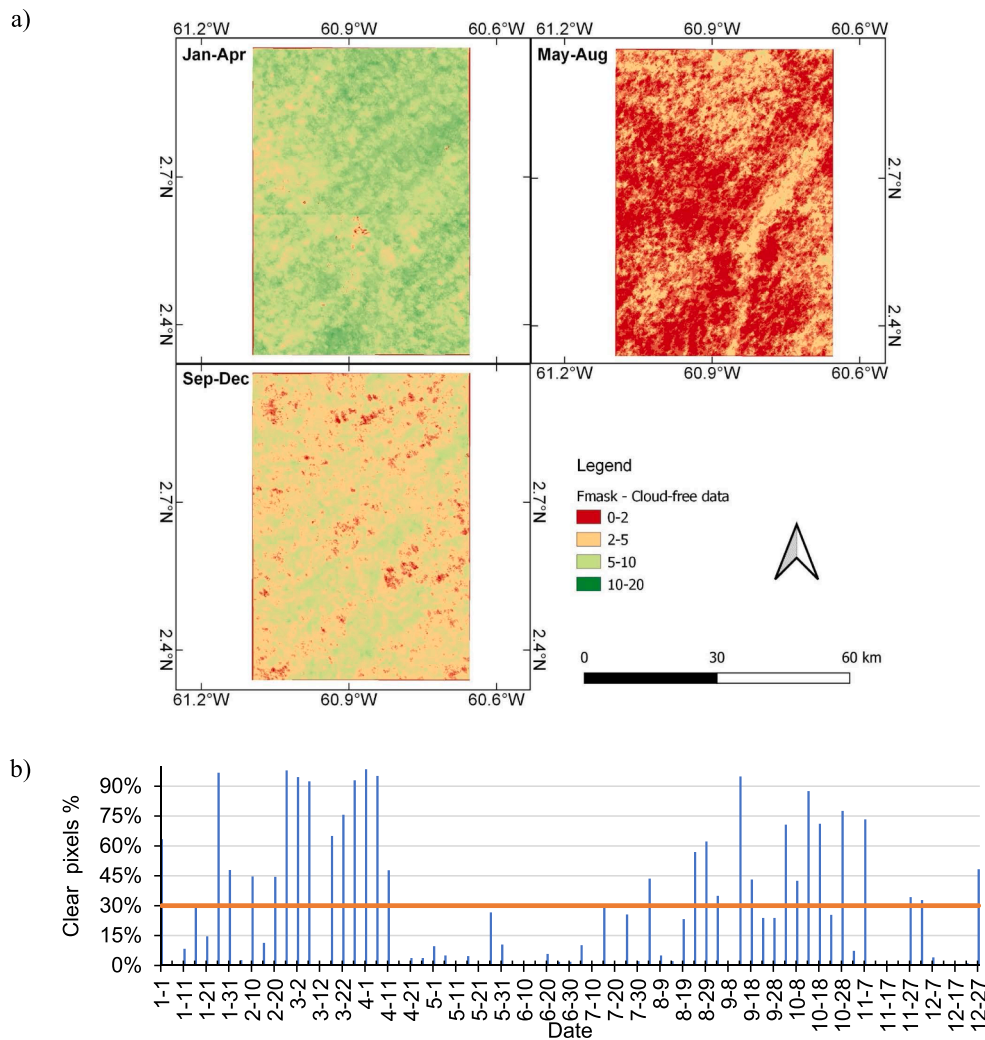


Fig. 4. Cloud-free pixels considering three periods of 2019 (January to April, May to August, and September to December) (a) and graph with the cloud-free percentage for each image (b) over the study area for MSI data, using Fmask products.

Table 1
Input data combinations with Sentinel-1 and Sentinel-2.

Data	Bands/Polarization	Inputs
S2 Bands metrics	Blue, Green, Red, Red-edge 1, Red-edge 2, Red-edge 3, NIR, NIR-A, SWIR 1, and SWIR 2	average, median, standard deviation, variance, range, and percentiles (25%, and 75%)
S2 VI metrics	S2 VI metrics: NDVI, LSWI;	average, median, standard deviation, variance, range, and percentiles (25%, and 75%)
S1 polarization metrics	VV, VH, and ratio	only backscattering values
S1 polarization	VV, VH, and ratio	average, median, standard deviation, variance, range, and percentiles (25%, and 75%)

S2: Sentinel-2. S1: Sentinel-1, VI: Vegetation Indices.

errors. However, the OA confidence interval is indicated for randomness data (Olofsson et al., 2014; Stehman, 2012), and our estimation has limitations as the confidence interval was calculated based on data randomly selected from purposive sampling. Yet, we expected that the errors were uniform for all scenarios, once they were based on the same approach, allowing the comparison among them.

To use independent validation for the best classification result (scenario and classifier), we used Stratified Random Points (SRP). The goal of SRP is to have a practical design that satisfies the accuracy

Table 2
Details about the 29 scenarios formed with different datasets and periods.

Datasets	Input data	Periods
D1	S2 Bands metrics	P1, P2, P3, P4, P5
D2	S2 Bands metrics S2 VI metrics	P1, P2, P3, P4, P5
D3	S2 Bands metrics S2 VI metrics	P1, P2, P3, P4, P5
D4	S1 polarization metrics S2 Bands metrics S2 VI metrics	P1, P2, P3, P4, P5
D5	S1 polarization S1 polarization metrics	P1, P2, P3, P4, P5
D6	S1 polarization	P1, P2, P3, P4

S2: Sentinel-2. S1: Sentinel-1, VI: Vegetation Indices, P1: period 1 (January to April), P2: period 2 (May to August), P3: period 3 (September to December), P4: period 4 (the whole year), P5: period 5 (the periods P1, P2, and P3 combined).

measurement objectives and most of the desirable design criteria. SRP affords the option to increase the sample size in classes that occupy a small proportion of the area, to reduce the standard errors of the class-specific accuracy estimates for these rare classes (Olofsson et al., 2014). We calculated the area weight and the standard errors for the best classification result (with 10 m pixel), and after randomly sampling

1,158 points, stratified according to Forest: 262, Savannas: 272, Campinarana: 75, Water: 75, Pasture: 99, Sand/rocks: 75, Annual Crops: 75, Perennial Crops: 75, Conversion: 75, and Impermeable: 75. This guarantees that the sample size in a small class will be large enough to represent that class. This approach allows us to estimate the errors in terms of the area along with uncertainties.

2.6. Comparison with LULC map of MapBiomias

To verify where our approach could be helpful, we compared our best LULC classification results with MapBiomias Project. MapBiomias is the most recent initiative of the LULC mapping in Brazil (Souza et al., 2020), and is the only regularly updated LULC program that maps the whole Roraima State. It provides annual LULC maps for the entire country, between 1985 and 2019 (version 5). MapBiomias process uses the Google Earth Engine platform (Gorelick et al., 2017), Operational Land Imager (OLI), Enhanced Thematic Mapper Plus (ETM +), and Thematic Mapper (TM) Landsat optical images at 30 m spatial resolution. They do a hierarchical classification scheme using a Random Forest classifier and combine different classification methods (date range, input data, etc.) (Souza et al., 2020). It classified each LULC class separately and joined them, generating three different LULC map levels.

We used the MapBiomias version 5, Level 3, the year 2019. For our study area, our map has more detailed classes than MapBiomias Level 3. Thus, to analyze the differences between our classes, we harmonized the LULC classes between our LULC product and the MapBiomias product (Table 3). From MapBiomias, we combined Soybeans and Others Temporary Crops as Temporary Crops to compare with our Annual Crops. Sand/rocks and Conversion areas classes are not present in MapBiomias legend. Grassland Formations class in Mapbiomas represents our Savannas and Campinarana classes.

3. Results

In this section, we present first the results of input features visualization using the t-SNE algorithm (section 3.1). In section 3.2, we analyze classification results for the 29 different scenarios and the accuracy of the Stratified Random Points (SRP) of the final map.

3.1. Visualization of input features using t-SNE

We used t-SNE graphs to represent differences between the classes for each database in each period (Figure A1). When using only optical data, we observed better separation of the classes Forest, Savanna, and Pasture. For SAR, we could not verify the same separation as in the optical data. Classes with similar geometrical structures are closer or even mixed. We found that Forest and Perennial Crops are mixed, meanwhile, Savannas and Pasture represent two other groups, which have mixed with Annual Crops, Conversion areas.

Considering the periods and datasets, we found that the t-SNE technique showed better results for P4, data from the entire year, and

Table 3
Harmonized LULC classes to compare our LULC product with the MapBiomias project (version 5).

LULC class	MapBiomias LULC class
Forest	Forest Formation
Savannas	Grassland Formation
Campinarana	Grassland Formation
Water	River, Lake, and Ocean
Pasture	Pasture
Sand/rocks	
Annual Crops	Temporary crops: soybean and other temporary crops
Perennial Crops	Forest Plantation
Conversion areas	
Impermeable Areas	Urban Infrastructure

P5, combined P1, P2, and P3, and when combining data from optical and SAR sensors (D3 and D4) (Figure A1). Scenario D3P5 (Fig. 5) has the best visual results, with better separation to Forest, Savanna, Pasture, and Annual Crops classes. Perennial Crops class showed confusion with Forest, Savanna, and Pasture classes. Besides, Pasture has overlapped with Savannas and Annual Crops classes, and Campinarana was confused with Pasture. The Impermeable class is concentrated in the left-middle ($x = -8$; $y = -4$) of the graph (Fig. 5). Sand/rock has two small groups, one with Impermeable class and the other in the middle-bottom ($x = -1$; $y = -4$) of the graph.

3.2. LULC classification

The Overall Accuracy (OA) of all scenarios for MLP and RF classifiers is shown in Fig. 6, and the results from the confidence interval in Figure A3. In general, we verified that the MLP classifier showed higher OA than RF. Moreover, when using data from a single sensor, we found better results using optical data (D1 and D2) than SAR data (D5 and D6). For the periods analyzed, when we used data for the whole year (P4 and P5) we had higher accuracies than when using only data for P1 and P2. Considering the different periods of the year, the P2 has the lower and P3 has the higher OA values for optical data (D1 and D2). Meanwhile, for SAR datasets (D5 and D6) the higher value is for P2 and the lower for the P1. Finally, considering the multisensory SAR-optical approach (D3 and D4), we found that the OA values increased in almost all periods. Overall, the best result was achieved for the dataset D3, using data for the whole year P5, using MLP.

Users (UA) and Producers (PA) Accuracies were calculated for all scenarios using MLP (Figure A4) and RF (Figure A5) classifiers. Considering that the MLP approach has better overall accuracies, we showed the UA and the PA of this analysis in detail (Figure A4 and Figure A5). SAR dataset showed higher UA and PA for Savanna, Pasture, and Annual Crops, but lower UA and PA values for Campinarana and Conversion classes. In general, optical data has better results than SAR. However, the UA for Sand/rocks and Campinarana, and the PA for Conversion classes remain low. In general, when we combined features from optical and SAR (D3 and D4) accuracies (UA and PA) improved for Forest, Savannas, Annual Crops, and Perennial Crops classes (Figure A4 and Figure A5). These patterns were more evident when we integrated features from D3 and D4 for the entire year (P4) and different periods combined (P5). We also highlighted the better UA and PA values for P3

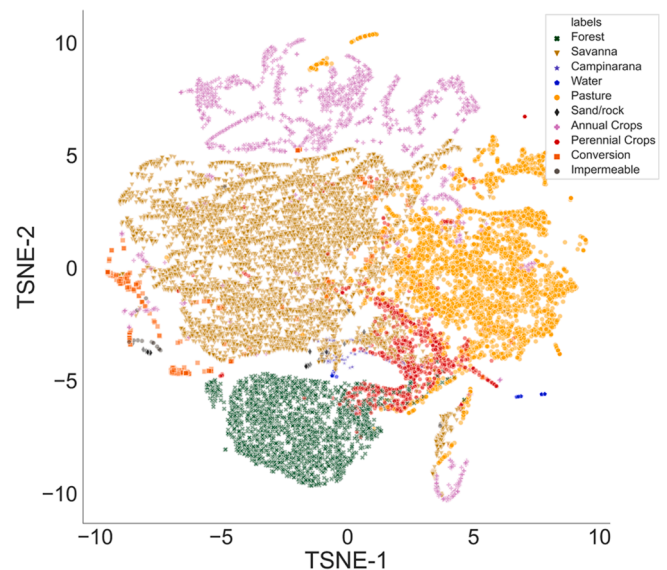


Fig. 5. t-SNE graph for the scenario with the best separation among LULC classes (D3P5).



Fig. 6. Overall Accuracy (OA) of the LULC classification using Random Forest (RF) and Multi-layer Perceptron (MLP) classifiers, using testing data for the scenarios analyzed.

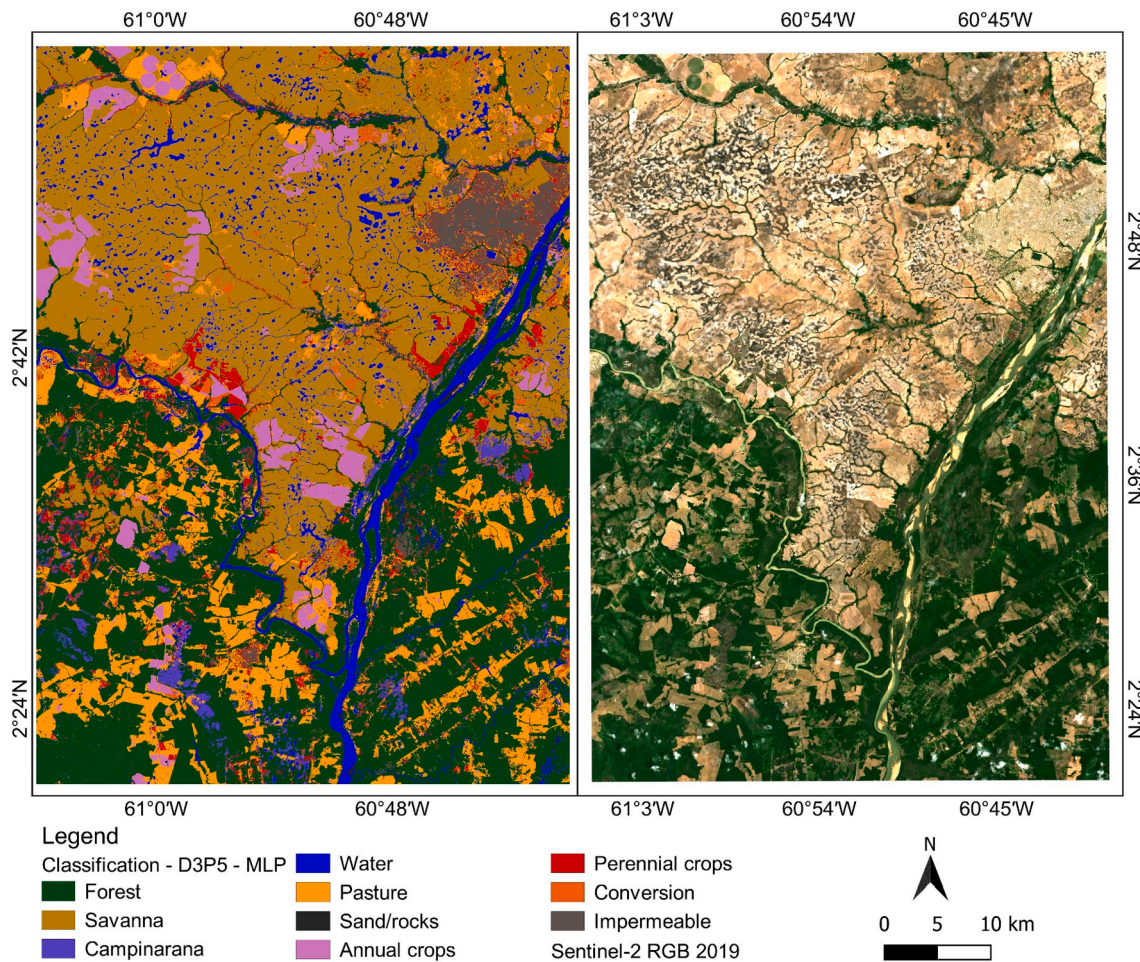


Fig. 7. Map for the best LULC classification scenario (D3P5), using the MLP classifier (left), and a 2019 Sentinel-2 RGB True color image, using the mean of the band values over the year (right).

compared to P2 and P1.

MLP (Figure A6) and RF (Figure A7) maps to all scenarios are heterogeneous. In general, maps based only on SAR data showed more salt-pepper effects, while maps based only on optical data presented cloud interference. The problems were reduced when the multisensor approach was employed. The best classification (Fig. 7) was obtained using optical metrics and SAR data (D3) combining data from the different periods (P5). The predominant class is Savannas (119,936 ha ~ 34.17%), followed by Forest (115,155 ha ~ 32.81%) and Pasture (43,309 ha ~ 12.34%). Perennial Crops (17,859 ha ~ 5.09%), Water (17,658 ha ~ 5.03%), and Annual crops (14,215 ha ~ 4.05%) are the following classes in terms of the mapped area. The classes with smallest area are Sand/rocks (1,700 ha ~ 0.48%), Conversion (2,347 ha ~ 0.67%), Impermeable (8,724 ha ~ 2.49%), and Campinarana (10,115 ha ~ 2.88%).

To further evaluate the LULC classification accuracy, we performed the accuracy assessment using an independent SRP. The OA accuracy estimated from SRP was $OA = 86.41 \pm 1.74\%$, reaching almost the same value from the field points ($OA = 88.15\%$). To compare the accuracies for each class, we provided confusion matrices (Fig. 8 and Fig. 9) along with estimated UA and PA (Fig. 10).

3.3. Comparison with MapBiomias LULC map

We compared our results with maps from the MapBiomias initiative (Souza et al., 2020), version 5 (Table 4). For our study area, MapBiomias LULC (Fig. 11) was classified as Forest Formation (116,875 ha ~ 32.95%), Forest Plantation (40 ha ~ 0.01%), Grassland Formation (166,925 ha ~ 47.06%), Pasture (43,086 ha ~ 12.15%), Urban Infrastructure (10,570 ha ~ 2.98%), River, Lake, and Ocean (7,336 ha ~ 2.07%) and Temporary Crops (9,910 ha ~ 2.79%). Temporary Crops on MapBiomias approach is formed for Soybean (7,522 ha ~ 2.12%) and

Others Temporary Crops (2,388 ha ~ 0.67%). The difference map between our approach and the MapBiomias initiative is shown in Fig. 12. The agreement area, considering Grassland formation equal to Savannas and Campinarana, is 277,083 ha (~79%) and the differences are 73,937 ha (~21%). We can highlight that part of Grassland formation in the MapBiomias LULC program is classified as Pasture (10,678 ha), Perennial crops (8,690 ha), Water (8,468 ha), Annual crops (5,091 ha), and Forest (4,719 ha) classes in our approach. Besides, part of our Forest (5,813 ha) classifications are mapped as Pasture in the MapBiomias product.

We identified areas with Acacia and Cashew (Perennial Crops) that were not present inside the Forest Plantation class in the MapBiomias LULC map. Acacia is a common Forest plantation in Roraima Lavrados, started in 2000, and now it has been converted into agricultural areas. Also, we have the Conversion class and this is an important class to identify where and when changes are occurring with transitions from a natural class to an anthropic activity. Sand/rocks and Conversion classes are not used in MapBiomias. Moreover, Sandbanks inside of the Rio Branco River are identified as Temporary Crops on MapBiomias map. Additionally, our results showed the Lakes formations in the Savannas regions. Therefore, our results provided a better overview of the natural resources, conversion areas, and land use, classifying all in a single step. This information is important to monitor and regulate anthropic activity; otherwise, it can affect the availability of natural resources (e.g. water, soil) (Carvalho and Mustin, 2017) and carbon stocks (Barni et al., 2016).

4. Discussion

In this section, first, we present a discussion about the LULC classes' separability of our database based on the t-SNE algorithm (section 4.1). After, we contextualized the results from the scenarios and classifiers analyzed (in section 4.2). In section 4.3 we discuss our best result and

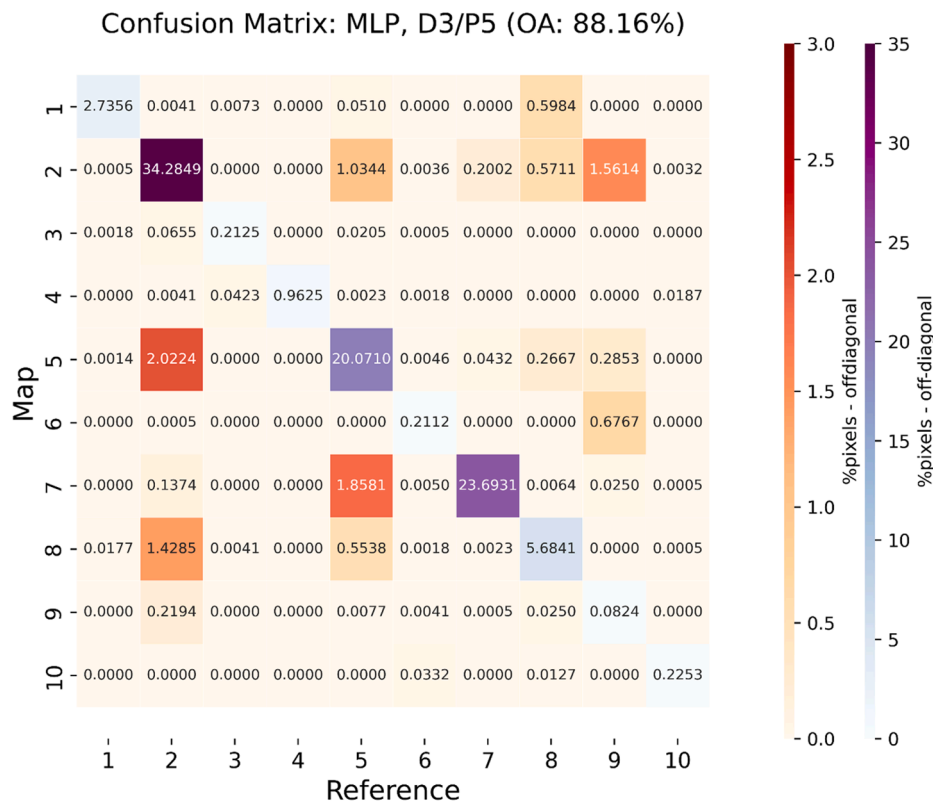


Fig. 8. Confusion matrix in terms of validation pixels from polygons derived through field campaign for the best LULC classification scenario (D3P5 – MLP), using field data. Values are in percentage (total number of samples wise). 1: Forest, 2: Savannas, 3: Campinarana, 4: Water, 5: Pasture, 6: Sand/rocks, 7: Annual Crops, 8: Perennial Crops, 9: Conversion areas, 10: Impermeable areas.

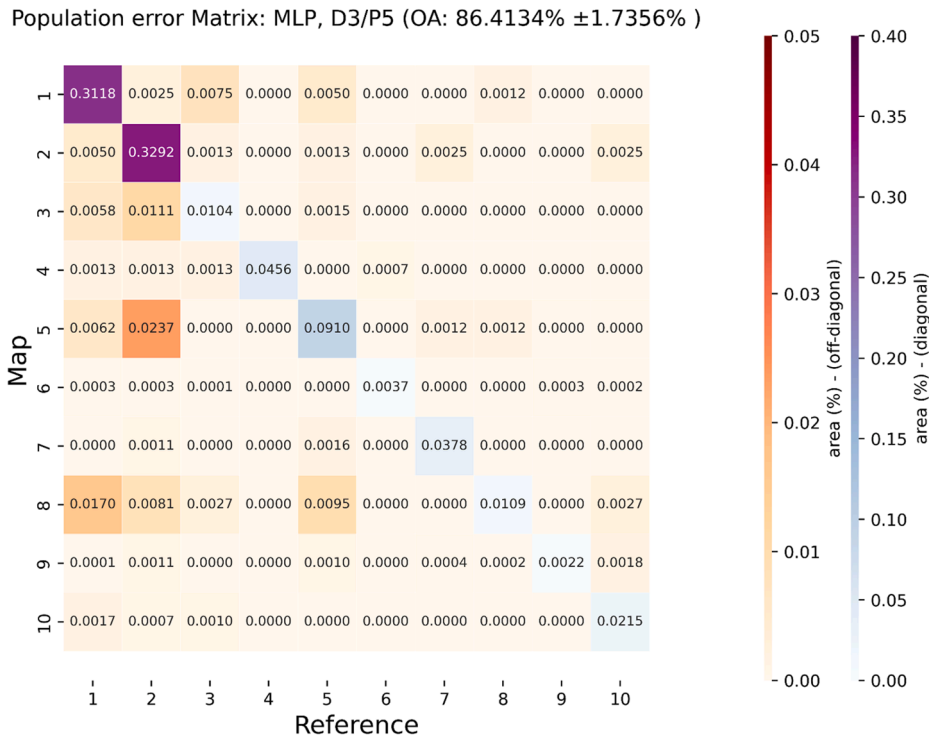


Fig. 9. Population error matrix in terms of proportion of area (Olofsson et al., 2014) for the best LULC classification scenario (D3P5 – MLP), using Stratified Random Points. Labels meaning, see Fig. 8.

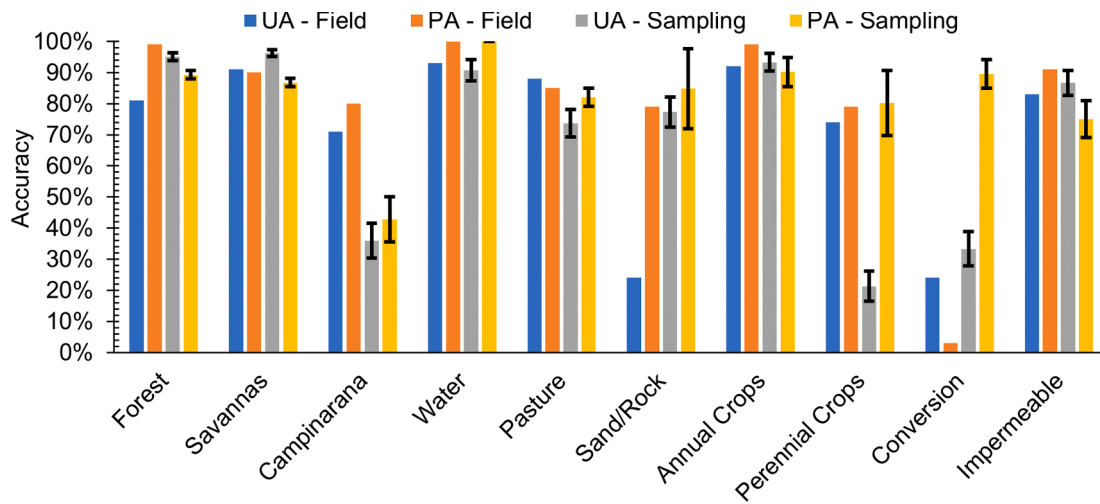


Fig. 10. Comparison among LULC classification accuracies from testing data and SRP approach.

compare it with the LULC map of MapBiomass.

4.1. t-SNE visualization

Before the classification process, we used the t-SNE (t-Distributed Stochastic Neighbor Embedding) technique to visualize how the different scenarios (combination of the datasets and periods, as described in Table 2) could provide the LULC classes separability. In general, t-SNE showed that the optical dataset performed a better visual separation than SAR datasets. With t-SNE it was possible to identify that the best visual separation among the classes happens with SAR-optical data (D3), combining the three different periods (P5), scenario D3P5. In this sense, our study shows that t-SNE provides a good way to visualize high dimensionality RS data than classic techniques, such as scatter

plots (Pavanelli et al., 2018) and boxplots (Torbick et al., 2017a, 2016), and can be used to analyze the potential of different datasets for class separation before the classification process. However, only a few studies have used this technique in the RS field (Dey et al., 2020; Martins et al., 2020), and we did not find any research that applied the t-SNE in a multisensor dataset.

4.2. Scenarios and classifiers

Our results have suggested that combining SAR and optical data, along different periods, allowed us to accurately map Land Use and Land Cover (LULC) in the Roraima state, in Brazil. This region is prone to periods of frequent cloud cover during the April-August (P2, rainy season), which severely limited the exploitation of optical satellite imagery.

Table 4

Comparison between the areas from our LULC product with the MapBiomass LULC map(version 5).

LULC product	Area (ha)	%	MapBiomass LULC class	Area (ha)	%
Forest	115,155	32.81	Forest Formation	116,875	32.95
Savannas	119,936	34.17	Grassland Formation	166,925	47.06
Campinarana	10,115	2.88			
Water	17,658	5.03	River, Lake, and Ocean	7,336	2.07
Pasture	43,309	12.34	Pasture	43,086	12.15
Sand/rocks	1,700	0.48	–	–	–
Annual Crops	14,215	4.05	Temporary crops: soybean and other temporary crops	9,910	2.79
Perennial Crops	17,859	5.09	Forest Plantation	40	0.01
Conversion areas	2,347	0.67	–	–	–
Impermeable Areas	8,724	2.49	Urban Infrastructure	10,570	2.98

Moreover, our approach achieved better results than the existing LULC programs, e.g. MapBiomass (as shown in Fig. 11). In this context, we believe that this study can be an alternative to improve the LULC classification. Therefore, the optical-SAR multisensor approach is a viable alternative to provide LULC classification in regions with frequent cloud cover. To validate this, we used two different classifiers algorithms in 29 scenarios, with optical only, SAR only, and SAR-optical datasets, within five different periods of the year 2019.

We used the RF, commonly used in a multisensor SAR-optical approach to map LULC (Clerici et al., 2017; Pavanelli et al., 2018; Torbick et al., 2017a, 2016; Zhou et al., 2017) and the MLP classifier for each one of the 29 scenarios. Using Sentinel-1 SAR data for LULC mapping over a test area in the Brazilian Amazon forest, de Diniz et al. (2020) achieved an OA result of 8.2% bigger using RF (OA = 82.7%) than Support Vector Machine (OA = 74.5%). It is important to highlight that a comparison between different classifications, in terms of overall accuracy, is meaningful when the number of classes mapped are similar. Since this is not the case here, we cannot directly compare Diniz et al. (2020) OA with ours. In our study, we found slightly higher OA values (1% or 2% in general) using MLP classifiers compared to RF (Fig. 6). Besides, LULC classifications from MLP were visually better, with less salt-pepper effect when compared with RF classifier. Considering the datasets analyzed (Fig. 6), we identified that aggregating VI metrics (D2) improves results than using MSI surface reflectance metrics only (D1). Also, the use of metrics for SAR data (D5) improves the OA when compared to SAR data only (D6). For SAR-optical data-based classifications, we found better overall accuracies than when analyzing SAR and optical data individually. In general, when we combined features from optical and SAR (D3 and D4), the Forest, Savannas, Annual Crops, and Perennial Crops classes are better discriminated. Besides, the LULC maps were visually better with the multisensor approach. Clerici et al. (2017) also found better results using optical (MSI/Sentinel-2) and SAR (Sentinel-1) data to map LULC in Colombia. They found that SVM (Support Vector Machine) had better accuracy than the RF classifier, achieving OA = 88.75%. Compared to our study, their study area was more homogeneous with six LULC classes. Zhou et al. (2017), using data from OLI/Landsat-8 and SAR/Sentinel-1 provided in-season winter wheat classification in China, achieved the best results with the multisensor approach. Torbick et al. (2016) integrated data from OLI/Landsat8, Sentinel-1, and PALSAR-2 images to map forest plantations in Myanmar and Indonesia. They got the best accuracy when integrating the data from the three sensors. In the following work, Torbick et al. (2017a) used data from the same sensors to classify/update the LULC in Myanmar, and also found the best accuracy using data from optical and SAR data combined.

Considering the periods analyzed, the classifications performed for

P3 had better results than for P1 and P2. That could be because during P2 we had less optical data available, resulting in a poor classification. Pavanelli et al. (2018) mentioned that the use of data only from the dry season is not enough to discriminate all LULC classes. Also, the fieldwork was realized at the end of P2 and the beginning of P3, helping to better identify some classes in the field. Pavanelli et al. (2018) and Lu et al. (2011), who worked with multisensor approaches to LULC classification in the Amazon regions, described the difficulty to get cloud-free data during the rainy season. However, they used only one optical and one SAR image from the dry season. Diniz et al. (2020) mentioned that using a time series SAR data could improve the LULC classification over a tropical region. We found that considering the data from January to December (P4), the classification based on SAR data (D5 and D6) had a better performance than optical data. That could be due to the cloud frequency limiting the optical data availability (Fig. 4) and thus the temporal variation from the classes could be better represented. We achieved better accuracy (OA = 88.16%) with the data from the P5, aggregating the data from P1 (January to April), P2 (May to August), and P3 (September to December). With this approach, the seasonality existing in the classes was considered in dry (part of the P3 and P1) and wet (P2) periods. For example, this approach allows us to explore the potential of SAR data during the wet period without giving up the potential of optical data for the dry period.

In our study, dynamic classes such as Sand/rocks, Water, and Conversion, are better discriminated in specific periods. Sand/rocks class was better identified in the dry period (P1) because the sandbanks appear inside the Rio Branco River in this period. The Water class, in general, had a better performance for P3, due to the end of the rainy season in P2, forming the small lakes in the lavrados regions, favoring the identification in the P3. During the P3, the Conversion class also had better discrimination, mainly because our fieldwork campaigns (section 2.1) were at beginning of the period. We expected that because conversion is a dynamic class, occurring during part of the year, thus some of these areas were Savannas or Pasture in a different period of the year. Besides, sometimes there is no vegetation for the Conversion class, creating confusion with the Sand/rocks class.

Due to the frequent cloud cover in the P2, the Annual Crops class was better discriminated with SAR than optical data. Besides, Pasture is present during this period and is a source of confusion between these classes. Forest, Savanna, Pasture, and Annual Crops classes were better discriminated when we used data from P4 and P5. That happens because the data for the entire year are being used, and as such it allows for capturing the vegetation variability and mitigating the cloud cover frequency interference on optical data with the use of the SAR (Prudente et al., 2020a). Perennial Crops is a heterogeneous class, formed by Acacias, Carswell, Eucalyptus, etc. Therefore, it was expected the confusion in this class with Forests and Savanna classes, due to the similar structure.

4.3. Best classification result

Overall, our best LULC classification accuracy over the 29 scenarios and two classifiers was obtained using the MLP classifier applied to the data from optical and SAR data combined (D3), considering the three periods together (P5). We used the benefits of optical and SAR data associated with the seasonality from different periods. We assessed the accuracy of this classification by performing Stratified Random Points (SRP). The approach with field data and SRP were similar in respect of overall accuracy, however, UA and PA values were different for Campinarana, Pasture, Perennial Crops, and Conversion classes. These classes have a spatial dependence on roads and are spectral and/or geometrical similar to other classes, being better represented with SRP.

Pavanelli et al. (2018) provided LULC classification in a small area with ecological tension between savannas and forests in Roraima. They considered 17 LULC classes for 2015 and used one OLI (Operational Land Imager) Landsat-8 optical image and one ALOS/PALSAR-2 (Phased

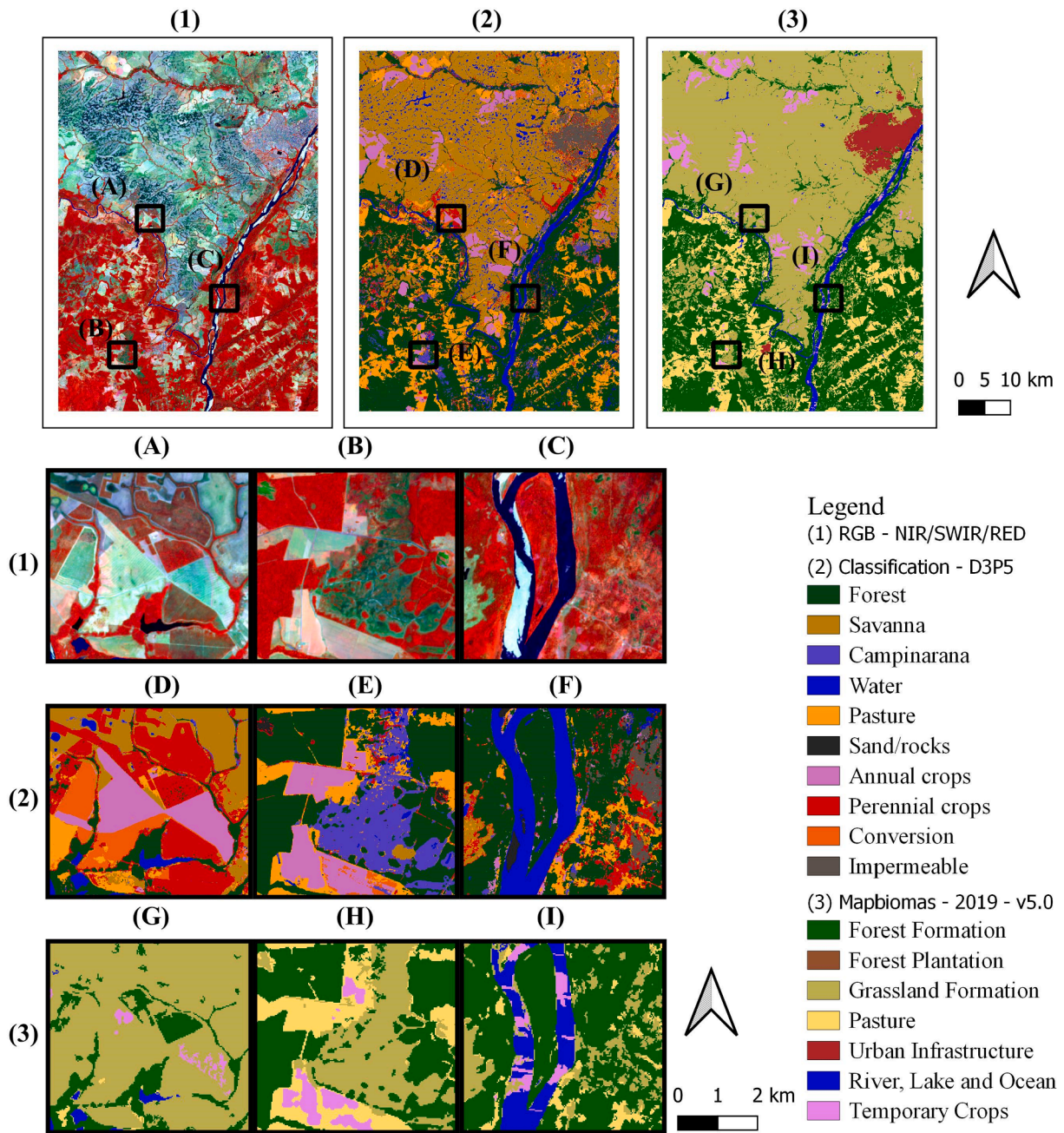


Fig. 11. Differences between our LULC mapping and the LULC provide for MapBiomass v5.0 – 2019 (Souza et al., 2020).

Array L-band Synthetic Aperture Radar-2) SAR image. They found an OA of 83% using RF classifier. Lu et al. (2011), using a Maximum Likelihood classifier, found a LULC map accuracy of OA = 81.13% using only optical data rather than SAR data or integrating SAR and optical data. The studied area was conducted in Para state, Brazil, with a predominance of the rainforest. Besides, they used only one image per sensor, ALOS PALSAR, RADARSAT-2, and TM/Landsat-5, during the dry season. These authors utilized data fusion approaches (principal component analysis, normalized multiplication, high-pass filter resolution-merging, and Wavelet) instead of the feature combined, and considered fewer LULC classes (Forest, Pasture, Water, Wetland, Urban, and Succession Vegetation). Different from the previous studies, our approach used images from different periods (P5) and combined the results at the feature level, allowing us to explore the potential of SAR and optical data. Our results with the MLP classifier showed a higher OA and a better visual map with 10 m of resolution. Also, in our study we

used free data, that was not fully available in the area in 2015 or before.

Finally, we compared our best result with the MapBiomass LULC map (Souza et al., 2020). In this sense, we believe that our results could be helpful to improve the next MapBiomass LULC version, mainly to better discriminate Annual Crops, Perennial Crops, and the Lakes formations LULC classes. As we expected, using SAR and optical data for different periods we increased the chances of representing the seasonality of the region. Meanwhile, MapBiomass, using only optical data for the entire year, could result in a few (or non) observations during the same period, having a smaller representation of the temporal variation. Due to the use of SAR data for the P2, we increase the number of observations and guarantee that the use of the metrics represents the Annual Crops variations. In that sense, using metrics for P1 and P3, we also avoid the misclassification of sandbanks as Annual Crops, once sandbanks appear during the dry season, P3 to P1. Combining these three periods also allowed us to capture the lakes' seasonality and better discriminate this

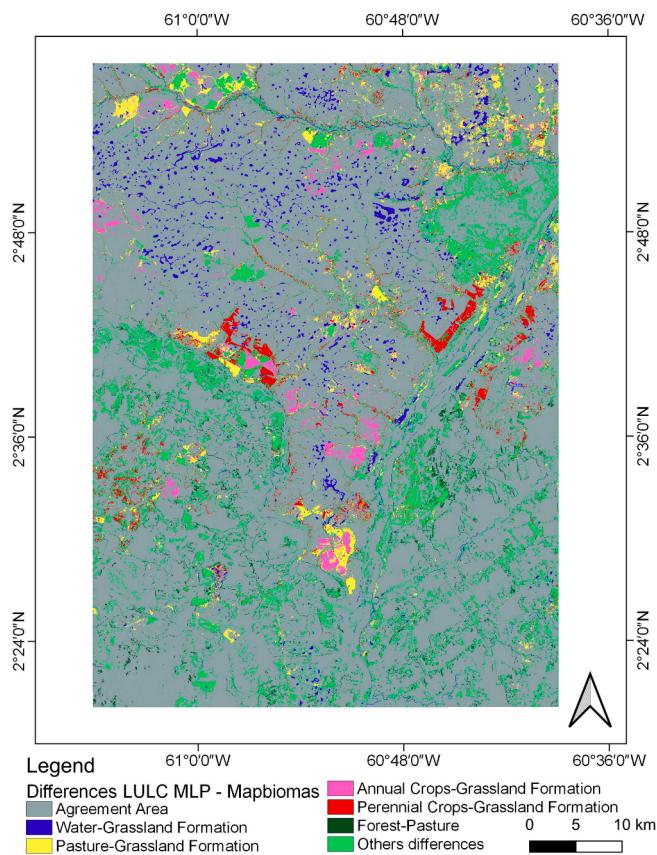


Fig. 12. Map of the differences between our LULC mapping and the LULC provide for MapBiomias v5.0 – 2019 (Souza et al., 2020).

class inside the lavrados regions. For Perennial Crops, as we are using SAR data, more sensitive to the canopy geometry, we have been more successful to discriminate the Acacias plantation inside the Perennial Crops than MapBiomias. However, it is important to highlight MapBiomias is a nationwide initiative, with annual LULC maps that are improving each version. Besides, we did not compare our results with other wide LULC programs as TerraClass Amazon (Almeida et al., 2016) and IBGE (IBGE, 2017). These approaches did not cover the Savannas and Campinarana regions (Barni et al., 2020b). They are classified as not observed in the TerraClass and as Grassland and Wetlands in IBGE. Moreover, these data have not been updated since 2014. Sentinel-1 has an important role to discriminate the LULC classes due to the frequent cloud cover in Roraima and consequently lack of cloud-free optical data. Consequently, combining SAR and optical, with data from different periods of the year, proved to be helpful to improve the LULC classification for Roraima.

5. Conclusions

Our approach represents an advancement for the heterogenous LULC mapping in the tropical region of Roraima with Earth remote sensing data. Optical and SAR multisensor data had better OA than optical or SAR data only. Besides, SAR data is an important source of data mainly during the rainy season (P2), when cloud cover limits the availability of useful optical imagery. The use of different periods allowed us to identify the optimal time for mapping land cover specific classes. SAR-optical data for the P5, combining P1 (January to April), P2 (May to August), and P3 (September to December), showed better performance. Moreover, the MLP classifier yielded higher OA than RF. Minor and mixed classes are difficult to distinguish, even with SAR and optical data. For future work, this approach could be applied to different areas

and different years to analyze the performance in other sites and the applicability to LULC changes analysis.

Declaration of Competing Interest

The authors declare that they have no known competing financial interests or personal relationships that could have appeared to influence the work reported in this paper.

Acknowledgments

This study was funded in part by the Coordenação de Aperfeiçoamento de Pessoal de Nível Superior - Brasil (CAPES) - Finance Code 001. The authors acknowledge the Conselho Nacional de Desenvolvimento Científico e Tecnológico (CNPq) for the Research Productivity Fellowship of I.D. Sanches (PQ - 303012/2018-8), and M. Adami (PQ - 306334/2020-8) and for V.H.R. Prudente doctorate scholarship. We appreciate the Embrapa Roraima fieldwork support by Dr. Haron Xaud and Dr. Maristela Xaud, through TERRAMZ (*Conhecimento Compartilhado para Gestão Territorial Local na Amazônia*) project.

Appendix A. Supplementary data

Supplementary data to this article can be found online at <https://doi.org/10.1016/j.isprsjprs.2022.04.025>.

References

- Adami, M., Bernardes, S., Arai, E., Freitas, R.M., Shimabukuro, Y.E., Espírito-Santo, F.D. B., Rudorff, B.F.T., Anderson, L.O., 2018. Seasonality of vegetation types of South America depicted by moderate resolution imaging spectroradiometer (MODIS) time series. *Int. J. Appl. Earth Obs. Geoinf.* 69, 148–163. <https://doi.org/10.1016/j.jag.2018.02.010>.
- Almeida, C.A. de, Coutinho, A.C., Esquerdo, J.C.D.M., Adami, M., Venturieri, A., Diniz, C. G., Dessay, N., Durieux, L., Gomes, A.R., 2016. High spatial resolution land use and land cover mapping of the Brazilian Legal Amazon in 2008 using Landsat-5/TM and MODIS data. *Acta Amaz.* 46, 291–302. <https://doi.org/10.1590/1809-4392201505504>.
- Asner, G.P., 2001. Cloud cover in Landsat observations of the Brazilian Amazon. *Int. J. Remote Sens.* 22, 3855–3862. <https://doi.org/10.1080/01431160010006926>.
- Barbosa, R.I., Bacelar-Lima, C.G., 2008. Notas sobre a diversidade de plantas e fitofisionomias em Roraima através do banco de dados do herbário INPA. *Amaz. Ciência Desenvolv.* 4, 131–154.
- Barbosa, R.I., Keizer, E., Pinto, F., 2010. Ecosistemas terrestres de Roraima: área e modelagem espacial da biomassa. In: Barbosa, R.I. (Ed.), *Roraima: Homem, Ambiente e Ecologia*. Femact, Boa Vista, pp. 347–368.
- Barni, P.E., Barbosa, R.I., Xaud, H.A.M., Xaud, M.R., Fearnside, P.M., 2020a. Precipitation in northern Amazonia: Spatial distribution in Roraima, Brazil. *Soc. Nat.* 32, 439–456. <https://doi.org/10.14393/SN-v32-2020-52769>.
- Barni, P.E., Manzi, A.O., Condé, T.M., Barbosa, R.I., Fearnside, P.M., 2016. Spatial distribution of forest biomass in Brazil's state of Roraima, northern Amazonia. *For. Ecol. Manage.* 377, 170–181. <https://doi.org/10.1016/j.foreco.2016.07.010>.
- Barni, P.E., Roraima, U.E. De, Manzi, A.O., Fearnside, P., 2020b. Simulated deforestation versus satellite data in Roraima, Northern Amazonia, Brazil. *Sustain. Debate* 11, 78–94. [10.18472/SustDeb.v11n2.2020.27493](https://doi.org/10.18472/SustDeb.v11n2.2020.27493).
- Breiman, L., 2001. Random Forests. *Mach. Learn.* 45, 5–32. <https://doi.org/10.1023/A:1010933404324>.
- Burger, H.C., Schuler, C.J., Harmeling, S., 2012. Image denoising: Can plain neural networks compete with BM3D?. In: 2012 IEEE Conference on Computer Vision and Pattern Recognition. IEEE, pp. 2392–2399. <https://doi.org/10.1109/CVPR.2012.6247952>.
- Camargo, F.F., Sano, E.E., Almeida, C.M., Mura, J.C., Almeida, T., 2019. A Comparative Assessment of Machine-Learning Techniques for Land Use and Land Cover Classification of the Brazilian Tropical Savanna Using ALOS-2/PALSAR-2 Polarimetric Images. *Remote Sens.* 11, 1600. <https://doi.org/10.3390/rs11131600>.
- Carvalho, W.D. de, Mustin, K., 2017. The highly threatened and little known Amazonian savannas. *Nat. Ecol. Evol.* 1, 0100. <https://doi.org/10.1038/s41559-017-0100>.
- Clerici, N., Valbuena Calderón, C.A., Posada, J.M., 2017. Fusion of Sentinel-1A and Sentinel-2A data for land cover mapping: a case study in the lower Magdalena region. *Colombia. J. Maps* 13, 718–726. <https://doi.org/10.1080/17445647.2017.1372316>.
- Cué La Rosa, L.E., Queiroz Feitosa, R., Nigri Happ, P., Del'Arco Sanches, I., Ostwald Pedro da Costa, G.A., 2019. Combining Deep Learning and Prior Knowledge for Crop Mapping in Tropical Regions from Multitemporal SAR Image Sequences. *Remote Sens.* 11 (17), 2029.

- Deng, X., Zhao, C., Yan, H., 2013. Systematic Modeling of Impacts of Land Use and Land Cover Changes on Regional Climate: A Review. *Adv. Meteorol.* 2013, 1–11. <https://doi.org/10.1155/2013/317678>.
- Dey, S., Mandal, D., Robertson, L.D., Banerjee, B., Kumar, V., McNairn, H., Bhattacharya, A., Rao, Y.S., 2020. In-season crop classification using elements of the Kennaugh matrix derived from polarimetric RADARSAT-2 SAR data. *Int. J. Appl. Earth Obs. Geoinf.* 88, 102059 <https://doi.org/10.1016/j.jag.2020.102059>.
- Diniz, J.M.F. de S., Gama, F.F., Adami, M., 2020. Evaluation of polarimetry and interferometry of sentinel-1A SAR data for land use and land cover of the Brazilian Amazon Region. *Geocarto Int.* 0, 1–19. [10.1080/10106049.2020.1773544](https://doi.org/10.1080/10106049.2020.1773544).
- Dong, J., Xiao, X., Chen, B., Torbick, N., Jin, C., Zhang, G., Biradar, C., 2013. Mapping deciduous rubber plantations through integration of PALSAR and multi-temporal Landsat imagery. *Remote Sens. Environ.* 134, 392–402. <https://doi.org/10.1016/j.rse.2013.03.014>.
- Eberhardt, I.D.R., Schultz, B., Rizzi, R., Sanches, I.D., Formaggio, A.R., Atzberger, C., Mello, M.P., Immitzer, M., Trabaquini, K., Foschiera, W., Luiz, A.J.B., 2016. Cloud cover assessment for operational crop monitoring systems in tropical areas. *Remote Sens.* 8, 1–14. <https://doi.org/10.3390/rs8030219>.
- ESA, E.S.A., 2020. MultiSpectral Instrument (MSI) Overview [WWW Document]. Tech. Guid. - Sentinel - 2 MSI. URL <https://earth.esa.int/web/sentinel/technical-guides/sentinel-2-msi/msi-instrument> (accessed 9.16.20).
- Estes, L.D., Searchinger, T., Spiegel, M., Tian, D., Sichinga, S., Mwale, M., Kehoe, L., Kuemmerle, T., Berven, A., Chaney, N., Sheffield, J., Wood, E.F., Caylor, K.K., 2016. Reconciling agriculture, carbon and biodiversity in a savannah transformation frontier. *Philos. Trans. R. Soc. B Biol. Sci.* 371 (1703), 20150316.
- Gómez, M.G.C., 2017. Joint use of Sentinel-1 and Sentinel-2 for land cover classification: A machine learning approach. Lund University.
- Gorelick, N., Hancher, M., Dixon, M., Ilyushchenko, S., Thau, D., Moore, R., 2017. Google Earth Engine: Planetary-scale geospatial analysis for everyone. *Remote Sens. Environ.* 202, 18–27. <https://doi.org/10.1016/j.rse.2017.06.031>.
- Harfenmeister, K., Spengler, D., Weltzien, C., 2019. Analyzing Temporal and Spatial Characteristics of Crop Parameters Using Sentinel-1 Backscatter Data. *Remote Sens.* 11, 1569. <https://doi.org/10.3390/rs11131569>.
- Harris, C.R., Millman, K.J., van der Walt, S.J., Gommers, R., Virtanen, P., Cournapeau, D., Wieser, E., Taylor, J., Berg, S., Smith, N.J., Kern, R., Picus, M., Hoyer, S., van Kerkwijk, M.H., Brett, M., Haldane, A., del Río, J.F., Wiebe, M., Peterson, P., Gérard-Marchant, P., Sheppard, K., Reddy, T., Weckesser, W., Abbasi, H., Gohlke, C., Oliphant, T.E., 2020. Array programming with NumPy. *Nature* 585 (7825), 357–362.
- Hu, J., Ghamisi, P., Zhu, X., 2018. Feature Extraction and Selection of Sentinel-1 Dual-Pol Data for Global-Scale Local Climate Zone Classification. *ISPRS Int. J. Geo-Information* 7, 379. <https://doi.org/10.3390/ijgi7090379>.
- Hu, L., He, S., Han, Z., Xiao, H., Su, S., Weng, M., Cai, Z., 2019. Monitoring housing rental prices based on social media: An integrated approach of machine-learning algorithms and hedonic modeling to inform equitable housing policies. *Land use policy* 82, 657–673. <https://doi.org/10.1016/j.landusepol.2018.12.030>.
- IBGE, I.B. de G. e E., 2018. Conheça cidades e estados do Brasil [WWW Document]. Bras. em síntese. URL <https://cidades.ibge.gov.br/brasil/rr/panorama> (accessed 7.19.18).
- IBGE, I.B. de G. e E., 2017. Monitoramento da cobertura e uso da terra do Brasil: 2000–2010–2012 – 2014: em grade territorial estatística, 1st ed. IBGE, Rio de Janeiro.
- IBGE, I.B. de G. e E., 2012. Manual Técnico da Vegetação Brasileira, 2nd ed. Rio de Janeiro.
- Inglada, J., Vincent, A., Arias, M., Marais-Sicre, C., 2016. Improved early crop type identification by joint use of high temporal resolution SAR and optical image time series. *Remote Sens.* 8 (5), 362.
- Jhonnier, R., Siregar, V.P., Nababan, B., Prasetyo, L.B., Wouthuyzen, S., 2015. Random Forest Classification for Mangrove Land Cover Mapping Using Landsat 5 TM and Alos Palsar Imageries. *Procedia Environ. Sci.* 24, 215–221. <https://doi.org/10.1016/j.proenv.2015.03.028>.
- Joshi, N., Baumann, M., Ehammer, A., Fensholt, R., Grogan, K., Hostert, P., Jepsen, M., Kuemmerle, T., Meyfroidt, P., Mitchell, E., Reiche, J., Ryan, C., Waske, B., 2016. A Review of the Application of Optical and Radar Remote Sensing Data Fusion to Land Use Mapping and Monitoring. *Remote Sens.* 8, 70. <https://doi.org/10.3390/rs8010070>.
- Lambin, E.F., Geist, H.J., Lepers, E., 2003. Dynamics of Land-Use and Land-Cover change in tropical regions. *Annu. Rev. Environ. Resour.* 28, 205–241. <https://doi.org/10.1146/annurev.energy.28.050302.105459>.
- Laurin, G.V., Liesenberg, V., Chen, Q., Guerriero, L., Del Frate, F., Bartolini, A., Coomes, D., Wilebore, B., Lindsell, J., Valentini, R., 2013. Optical and SAR sensor synergies for forest and land cover mapping in a tropical site in West Africa. *Int. J. Appl. Earth Obs. Geoinf.* 21, 7–16. <https://doi.org/10.1016/j.jag.2012.08.002>.
- Liu, C., Shang, J., Vachon, P.W., McNairn, H., 2013. Multiyear Crop Monitoring Using Polarimetric RADARSAT-2 Data. *IEEE Trans. Geosci. Remote Sens.* 51, 2227–2240. <https://doi.org/10.1109/TGRS.2012.2208649>.
- Lu, D., Batistella, M., Li, G., Moran, E., Hetrick, S., Freitas, C.d.C., Dutra, L.V., Sant’Anna, S.J.S., 2012. Land use/cover classification in the Brazilian Amazon using satellite images. *Pesqui. Agropecuária Bras.* 47 (9), 1185–1208.
- Lu, D., Li, G., Moran, E., Dutra, L., Batistella, M., 2011. A Comparison of Multisensor Integration Methods for Land Cover Classification in the Brazilian Amazon. *GIScience Remote Sens.* 48, 345–370. <https://doi.org/10.2747/1548-1603.48.3.345>.
- Maaten, L. Van Der, 2014. Accelerating t-SNE using Tree-Based Algorithms. *J. Mach. Learn. Res.* 15, 3221–3245.
- Martins, V.S., Kaleita, A.L., Gelder, B.K., Nagel, G.W., Maciel, D.A., 2020. Deep neural network for complex open-water wetland mapping using high-resolution WorldView-3 and airborne LiDAR data. *Int. J. Appl. Earth Obs. Geoinf.* 93, 102215 <https://doi.org/10.1016/j.jag.2020.102215>.
- Martins, V.S., Novo, E.M.L.M., Lyapustin, A., Aragão, L.E.O.C., Freitas, S.R., Barbosa, C. C.F., 2018. Seasonal and interannual assessment of cloud cover and atmospheric constituents across the Amazon (2000–2015): Insights for remote sensing and climate analysis. *ISPRS J. Photogramm. Remote Sens.* 145 <https://doi.org/10.1016/j.isprsjprs.2018.05.013>.
- Mlavec, J., Mlavcová, H., 2019. Locus Map Pro.
- Moreira, A., Prats-Iraola, P., Younis, M., Krieger, G., Hajnsek, I., Papathanassiou, K.P., 2013. A Tutorial on Synthetic Aperture Radar. *IEEE Geosci. Remote Sens. Mag.* 1 (1), 6–43.
- Nasirzadehdizaji, R., Sanli, F.B., Cakir, Z., Sertel, E., 2019. Crop Mapping Improvement by Combination of Optical and SAR datasets. In: in: 2019 8th International Conference on Agro-Geoinformatics (Agro-Geoinformatics). IEEE, pp. 1–6. <https://doi.org/10.1109/Agro-Geoinformatics.2019.8820604>.
- Oldoni, L.V., Prudente, V.H.R., Diniz, J.M.F.S., Wiederkkehr, N.C., Sanches, I.D., Gama, F. F., 2020. Polarimetric SAR data from Sentinel-1A applied to early crop classification. *ISPRS - Int. Arch. Photogramm. Remote Sens. Spat. Inf. Sci. XLIII-B3-2*, 1039–1046. <https://doi.org/10.5194/isprs-archives-XLIII-B3-2020-1039-2020>.
- Olofsson, P., Foody, G.M., Herold, M., Stehman, S.V., Woodcock, C.E., Wulder, M.A., 2014. Good practices for estimating area and assessing accuracy of land change. *Remote Sens. Environ.* 148, 42–57. <https://doi.org/10.1016/j.rse.2014.02.015>.
- Pavanelli, J.A.P., dos Santos, J.R., Galvão, L.S., Xaud, M.R., Xaud, H.A.M., 2018. PALSAR-2/ALOS-2 and OLI/Landsat-8 data integration for land use and land cover mapping in Northern Brazilian Amazon. *Bol. Ciências Geodésicas* 24, 250–269. <https://doi.org/10.1590/S1982-21702018000200017>.
- Pedregosa, F., Varoquaux, G., Gramfort, A., Michel, V., Thirion, B., Grisel, O., Blondel, M., Prettenhofer, P., Weiss, R., Dubourg, V., Vanderplas, J., Passos, A., Cournapeau, D., Brucher, M., Perrot, M., Duchesnay, É., 2011. Scikit-learn: Machine Learning in Python. *J. Mach. Learn. Res.* 12, 2825–2830. <https://doi.org/10.1007/s13398-014-0173-7.2>.
- Pohl, C., Van Genderen, J.L., 1998. Multisensor image fusion in remote sensing: Concepts, methods and applications. *Int. J. Remote Sens.* 19, 823–854. <https://doi.org/10.1080/014311698215748>.
- Prudente, V.H.R., Martins, V.S., Vieira, D.C., Silva, N.R.d.F.e., Adami, M., Sanches, I.D., 2020a. Limitations of cloud cover for optical remote sensing of agricultural areas across South America. *Remote Sens. Appl. Soc. Environ.* 20, 100414.
- Prudente, V.H.R., Sanches, I.D., Adami, M., Skakun, S., Oldoni, L.V., Xaud, H.A.M., Xaud, M.R., Zhang, Y., 2020b. SAR Data for Land Use Land Cover Classification in a Tropical Region with Frequent Cloud Cover. In: in: IGARSS 2020–2020 IEEE International Geoscience and Remote Sensing Symposium. IEEE, Hawaii, pp. 4100–4103. <https://doi.org/10.1109/IGARSS39084.2020.9323404>.
- Qiu, S., Zhu, Z., He, B., 2019. Fmask 4.0: Improved cloud and cloud shadow detection in Landsats 4–8 and Sentinel-2 imagery. *Remote Sens. Environ.* 231, 111205 <https://doi.org/10.1016/j.rse.2019.05.024>.
- Reiche, J., Hamunyela, E., Verbesselt, J., Hoekman, D., Herold, M., 2018. Improving near-real time deforestation monitoring in tropical dry forests by combining dense Sentinel-1 time series with Landsat and ALOS-2 PALSAR-2. *Remote Sens. Environ.* 204, 147–161. <https://doi.org/10.1016/j.rse.2017.10.034>.
- Reiche, J., Souza, C.M., Hoekman, D.H., Verbesselt, J., Persaud, H., Herold, M., 2013. Feature Level Fusion of Multi-Temporal ALOS PALSAR and Landsat Data for Mapping and Monitoring of Tropical Deforestation and Forest Degradation. *IEEE J. Sel. Top. Appl. Earth Obs. Remote Sens.* 6, 2159–2173. <https://doi.org/10.1109/JSTARS.2013.2245101>.
- Rodriguez-Galiano, V.F., Ghimire, B., Rogan, J., Chica-Olmo, M., Rigol-Sanchez, J.P., 2012. An assessment of the effectiveness of a random forest classifier for land-cover classification. *ISPRS J. Photogramm. Remote Sens.* 67, 93–104. <https://doi.org/10.1016/j.isprsjprs.2011.11.002>.
- Roraima, G. do E. de R., 2018. Investa em Roraima: Terra de oportunidades [WWW Document]. Investa em Roraima. URL <http://www.investaemroraima.rr.gov.br/site/?governoderoraima=ondeinvestir> (accessed 7.9.18).
- Rouse, J.W., Hass, R.H., Schell, J.A., Deering, D.W., 1973. Monitoring vegetation systems in the great plains with ERTS. *Third Earth Resour. Technol. Symp.* 1.
- Sano, E.E., Ferreira, L.G., Asner, G.P., Steinke, E.T., 2007. Spatial and temporal probabilities of obtaining cloud-free Landsat images over the Brazilian tropical savanna. *Int. J. Remote Sens.* 28, 2739–2752. <https://doi.org/10.1080/01431160600981517>.
- Searchinger, T.D., Estes, L., Thornton, P.K., Beringer, T., Notenbaert, A., Rubenstein, D., Heimlich, R., Licker, R., Herrero, M., 2015. High carbon and biodiversity costs from converting Africa’s wet savannahs to cropland. *Nat. Clim. Chang.* 5, 481–486. <https://doi.org/10.1038/nclimate2584>.
- Skakun, S., Kussul, N., Shelestov, A.Y., Lavreniuk, M., Kussul, O., 2016. Efficiency Assessment of Multitemporal C-Band Radarsat-2 Intensity and Landsat-8 Surface Reflectance Satellite Imagery for Crop Classification in Ukraine. *IEEE J. Sel. Top. Appl. Earth Obs. Remote Sens.* 9, 3712–3719. <https://doi.org/10.1109/JSTARS.2015.2454297>.
- Skakun, S., Roger, J.-C., Vermote, E.F., Masek, J.G., Justice, C.O., 2017. Automatic sub-pixel co-registration of Landsat-8 Operational Land Imager and Sentinel-2A Multi-Spectral Instrument images using phase correlation and machine learning based mapping. *Int. J. Digit. Earth* 10, 1253–1269. <https://doi.org/10.1080/17538947.2017.1304586>.
- Souza, C.M., Z. Shimbo, J., Rosa, M.R., Parente, L.L., A. Alencar, A., Rudorff, B.F.T., Hasenack, H., Matsumoto, M., G. Ferreira, L., Souza-Filho, P.W.M., de Oliveira, S.W., Rocha, W.F., Fonseca, A.V., Marques, C.B., Diniz, C.G., Costa, D., Monteiro, D., Rosa, E.R., Vêlez-Martin, E., Weber, E.J., Lenti, F.E.B., Paternost, F.F., Pareyn, F.G. C., Siqueira, J.V., Viera, J.L., Neto, L.C.F., Saraiva, M.M., Sales, M.H., Salgado, M.P.

- G., Vasconcelos, R., Galano, S., Mesquita, V.V., Azevedo, T., 2020. Reconstructing Three Decades of Land Use and Land Cover Changes in Brazilian Biomes with Landsat Archive and Earth Engine. *Remote Sens.* 12 (17), 2735.
- Steele-Dunne, S.C., McNairn, H., Monsivais-Huertero, A., Judge, J., Liu, P.-W., Papathanassiou, K., 2017. Radar Remote Sensing of Agricultural Canopies: A Review. *IEEE J. Sel. Top. Appl. Earth Obs. Remote Sens.* 10, 2249–2273. <https://doi.org/10.1109/JSTARS.2016.2639043>.
- Stehman, S.V., 2012. Impact of sample size allocation when using stratified random sampling to estimate accuracy and area of land-cover change. *Remote Sens. Lett.* 3, 111–120. <https://doi.org/10.1080/01431161.2010.541950>.
- Tamm, T., Zalite, K., Voormansik, K., Talgre, L., 2016. Relating Sentinel-1 Interferometric Coherence to Mowing Events on Grasslands. *Remote Sens.* 8, 802. <https://doi.org/10.3390/rs8100802>.
- The pandas development team, 2020. pandas-dev/pandas: Pandas 1.3.4 [WWW Document]. pandas-dev/pandas: Pandas. URL <https://zenodo.org/record/5574486#.YaAG37rQ9D9>.
- Torbick, N., Chowdhury, D., Salas, W., Qi, J., 2017a. Monitoring Rice Agriculture across Myanmar Using Time Series Sentinel-1 Assisted by Landsat-8 and PALSAR-2. *Remote Sens.* 9, 119. <https://doi.org/10.3390/rs9020119>.
- Torbick, N., Ledoux, L., Salas, W., Zhao, M., 2016. Regional Mapping of Plantation Extent Using Multisensor Imagery. *Remote Sens.* 8, 236. <https://doi.org/10.3390/rs8030236>.
- Torbick, N., Salas, W., Chowdhury, D., Ingraham, P., Trinh, M., 2017b. Mapping rice greenhouse gas emissions in the Red River Delta. *Vietnam. Carbon Manag.* 8, 99–108. <https://doi.org/10.1080/17583004.2016.1275816>.
- Torres, R., Snoeij, P., Geudtner, D., Bibby, D., Davidson, M., Attema, E., Potin, P., Rommen, B., Floury, N., Brown, M., Traver, I.N., Deghaye, P., Duesmann, B., Rosich, B., Miranda, N., Bruno, C., L'Abbate, M., Croci, R., Pietropaolo, A., Huchler, M., Rostan, F., 2012. GMES Sentinel-1 mission. *Remote Sens. Environ.* 120, 9–24. <https://doi.org/10.1016/j.rse.2011.05.028>.
- Van Der Maaten, L., Hinton, G., 2008. Visualizing data using t-SNE. *J. Mach. Learn. Res.* 9, 2579–2625.
- Van Tricht, K., Gobin, A., Gilliams, S., Piccard, I., 2018. Synergistic Use of Radar Sentinel-1 and Optical Sentinel-2 Imagery for Crop Mapping: A Case Study for Belgium. *Remote Sens.* 10, 1642. <https://doi.org/10.3390/rs10101642>.
- Veloso, A., Mermoz, S., Bouvet, A., Le Toan, T., Planells, M., Dejoux, J.F., Ceschia, E., 2017. Understanding the temporal behavior of crops using Sentinel-1 and Sentinel-2-like data for agricultural applications. *Remote Sens. Environ.* 199, 415–426. <https://doi.org/10.1016/j.rse.2017.07.015>.
- Whitcraft, A.K., McNairn, H., Lemoine, G., Letoan, T., Sobue, S., 2016. The Power of Synthetic Aperture Radar for Global Agricultural Monitoring. *Ceos*.
- Whitcraft, A.K., Vermote, E.F., Becker-Reshef, I., Justice, C.O., 2015. Cloud cover throughout the agricultural growing season: Impacts on passive optical earth observations. *Remote Sens. Environ.* 156, 438–447. <https://doi.org/10.1016/j.rse.2014.10.009>.
- Wulder, M.A., Hilker, T., White, J.C., Coops, N.C., Masek, J.G., Pflugmacher, D., Crevier, Y., 2015. Virtual constellations for global terrestrial monitoring. *Remote Sens. Environ.* 170, 62–76. <https://doi.org/10.1016/j.rse.2015.09.001>.
- Xiao, X., Boles, S., Liu, J., Zhuang, D., Liu, M., 2002. Characterization of forest types in Northeastern China, using multi-temporal SPOT-4 VEGETATION sensor data. *Remote Sens. Environ.* 82, 335–348. [https://doi.org/10.1016/S0034-4257\(02\)00051-2](https://doi.org/10.1016/S0034-4257(02)00051-2).
- Xiao, X., Hollinger, D., Aber, J., Goltz, M., Davidson, E.A., Zhang, Q., Moore, B., 2004. Satellite-based modeling of gross primary production in an evergreen needleleaf forest. *Remote Sens. Environ.* 89 (4), 519–534.
- Zhang, X., Wu, B., Ponce-Campos, G., Zhang, M., Chang, S., Tian, F., 2018. Mapping up-to-Date Paddy Rice Extent at 10 M Resolution in China through the Integration of Optical and Synthetic Aperture Radar Images. *Remote Sens.* 10, 1200. <https://doi.org/10.3390/rs10081200>.
- Zhang, Y., Skakun, S., Prudente, V., 2020. DETECTION OF CHANGES IN IMPERVIOUS SURFACE USING SENTINEL-2 IMAGERY. In: *IEEE International Geoscience and Remote Sensing Symposium*, pp. 4787–4790.
- Zhou, T., Pan, J., Zhang, P., Wei, S., Han, T., 2017. Mapping winter wheat with multi-temporal SAR and optical images in an urban agricultural region. *Sensors (Switzerland)* 17, 1–16. <https://doi.org/10.3390/s17061210>.